BBA - Molecular Cell Research 1868 (2021) 119080

Contents lists available at ScienceDirect

BBA - Molecular Cell Research

journal homepage: www.elsevier.com/locate/bbamcr

Peripheral IL-6/STAT3 signaling promotes beiging of white fat

Haifang Li [a,*,1], Mei Dong [a,1], Wenhui Liu [a,1], Cheng Gao [a], Yanxin Jia [a], Xinzhi Zhang [a], Xue Xiao [a], Qingxin Liu [a,*], Hai Lin [b,*]

[a] State Key Laboratory of Crop Biology, College of Life Sciences, Shandong Agricultural University, Tai'an 271018, China
[b] College of Animal Science and Veterinary Medicine, Shandong Agricultural University, Tai'an 271018, China

ARTICLE INFO

Keywords:
Interleukin-6 (IL-6)
Beiging of white fat
p-STAT3^{Tyr705}
PPARγ
UCP1

ABSTRACT

Interleukin-6 (IL-6) can reportedly centrally affect the thermogenesis of brown fat. However, whether the peripheral IL-6 signaling regulates beiging of white fat remains largely unknown. In vitro experiments indicated IL-6-KO-derived white adipocytes exhibited lower thermogenic gene expression compared to the WT, associating with reduced phosphorylation of STAT3 at Tyr705. Mechanistically, exogenous IL-6 application increased the p-STAT3^{Tyr705} level, thus the phosphorylated STAT3 bound to the promoter regions, and enhanced the transcription of *Pparγ* and *Ucp1*. The protein interaction of PGC-1α with PPARγ was increased by IL-6, which also contributed to stimulate *Ucp1* expression. In vivo experiments demonstrated that IL-6 KO decreased the beiging potential of white fat with suppressed STAT3 Tyr705 phosphorylation. Accordingly, IL-6-KO mature mice were associated with disrupted glucose homeostasis and accelerated hepatic steatosis. Collectively, we identified a novel function of peripheral IL-6/STAT3 signaling which is essential for beiging of white fat, such ensuring fat and glucose homeostasis.

1. Introduction

There are three functionally different types of fat in mammals: white, brown, and beige [1]. While white adipose tissue (WAT) mainly serves as a reservoir of triglycerides and secretes circulating factors that affect food intake or metabolism [1–4], brown adipose tissue (BAT) efficiently and beige fat in a less degree dissipate nutritional energy as heat via the uncoupling protein-1 (UCP1) [5,6]. Notably, beige adipocytes are derived from white fat under a process called of browning or beiging [6]. It has been established that metabolically active brown/beige fat is present in adult humans, and most is classified as more closely resembling beige adipocytes [7–9]. The abundance and activity of brown/beige fat positively correlate with leanness, higher insulin sensitivity, and improved complications caused by obesity [10,11].

Obesity is considered as a chronic low-grade inflammation, but the relationships between inflammation factors and obesity-related disorders are intricate and complex [12–15]. As one of the important interleukin family members, interleukin-6 (IL-6) has received much attention. IL-6 takes action through classical IL-6 signaling by receiving the signal via IL-6 receptor (IL-6R), or through IL-6 trans-signaling via soluble IL-6 receptor alpha (sIL-6Ra) [16]. Both endogenous and exogenous IL-6 has anti-obesity effects [17–20]. IL-6 deficient mice develop mature-onset obesity [21], show hepatic inflammation and systemic insulin resistance [22]. Xu et al. [23] reported that classical IL-6 signaling in T cells promotes inflammation and insulin resistance early during obesity development, but becomes dispensable at later stages, coinciding with a shift from classical T cell IL-6 signaling to enhanced IL-6 trans-signaling. Collectively, IL-6 seems to take pleiotropic effects on obesity development under different conditions, due to its classical- or trans-actions.

In addition, IL-6 works centrally to regulate BAT thermogenesis. Li et al. [24] demonstrated that central *Il-6* gene delivery increases the UCP1 protein level in BAT via sympathetic innervation. IL-6 microinjection into lateral parabrachial nucleus (LPBN) reduces food intake by interacting with leptin and enhances BAT thermogenesis by thyroid and sympathetic mechanisms [25]. However, whether and how peripheral IL-6 affects beiging of white fat remains largely unknown. Here we showed that IL-6 disruption inhibited, while exogenous IL-6 application stimulated, beiging of white adipocytes. Phosphorylation of signal transducer and activator of transcription 3 (STAT3) at Tyr705 was involved in IL-6 regulation of white adipocyte beiging, partially via enhancing the transcription of *Pparγ* and *Ucp1*. In vivo studies showed

* Corresponding authors.
E-mail addresses: haifangli@sdau.edu.cn (H. Li), liuqingxin@sdau.edu.cn (Q. Liu), hailin@sdau.edu.cn (H. Lin).
[1] The authors contributed equally to this work.

https://doi.org/10.1016/j.bbamcr.2021.119080
Received 19 January 2021; Received in revised form 3 June 2021; Accepted 13 June 2021
Available online 24 June 2021

that IL-6 KO decreased the beiging degree of white fat, associating with disrupted glucose homeostasis and accelerated hepatic steatosis. The present study uncovered a previously unrecognized facet of peripheral IL-6 signaling, which is essential for white fat beiging and protects against glucose imbalance and hepatic steatosis in mature mice.

2. Materials and methods

2.1. Animals and experimental protocol

All mice were on a C57BL/6J background. The IL-6 KO mice were purchased from the Jackson Laboratory (Bar Harbor, ME, USA). The mice were bred and housed at Shandong Agricultural University with constant environment on a standard 12:12 light cycle. Animals were allowed free access to water and standard laboratory chow diet, unless otherwise stated. The body weight and feed intake of mice were weekly recorded. At the end of the experiment, animals were kept fasting for 12 h and sacrificed by isoflurane inhalation followed by cervical dislocation. iWAT and iBAT from WT and KO mice were harvested and weighed. All studies were approved by the Animal Care and Use Committee of Shandong Agricultural University.

2.2. Isolation of white stromal vascular fraction cells (SVFs), in vitro differentiation and treatments

WAT in the inguen was isolated from 3-week-old mice by plastic and reconstructive surgery. The tissue was digested with 1.5 mg/mL collagenase I for 45 min at 37 °C, and white SVFs were obtained, as previously described [26]. The cells were cultured to subconfluence in basal medium containing 15% fetal bovine serum (FBS) and 1% penicillin/streptomycin. Subsequently, the WAT SVFs were induced to differentiate into white adipocytes using cocktail adipogenic stimuli (AS), consisting of 0.1 μM dexamethasone, 5 μg/mL insulin and 0.5 mM 3-isobutyl-1-methylxanthine (IBMX) for the first 2 days, and 0.1 μM dexamethasone and 5 μg/mL insulin for further 8 days. The media were replaced every 2 or 4 days. During the induced adipogenic process, 1 μM isoproterenol (ISO) (Selleck, USA) was used to stimulate the beiging process. Additionally, 10 ng/mL IL-6 (PeproTech, USA), 1 μM Niclosamide (Nic) (Selleck, USA), or 1 μM GW9662 (GW) (Selleck, USA) was individually or simultaneously supplemented into some cell culture dishes.

2.3. MitoTracker staining

Treated beige adipocytes were stained with MitoTracker Red CMXRos (200 nM) (CST, #9082) in DMEM containing 15% FBS at 37 °C for 30 min. Following washing twice with DMEM containing 15% FBS, the cells were incubated with DAPI (1 μg/mL) for 5 min at room temperature (RT). The intracellular MitoTracker-stained mitochondria were detected using a confocal laser scanning microscopy (CLSM) (Zeiss, Germany). Images were acquired and processed with the same setting for different treatments.

2.4. Immunofluorescence staining of UCP1

For immunofluorescence staining, Triton X 100-permeabilized beige adipocytes or adipose tissue slices cultured in climbing slices were pre-incubated with a blocking buffer (PBS containing 5% FBS) for 60 min, and incubated with UCP1 antibody (1:100 dilution) at 4 °C overnight. Subsequently, the slices were washed, and incubated with Alexa Flour 555-conjugated secondary antibody (1:500 dilution). After staining with DAPI (1 μg/mL) for 5 min, images were acquired by using a CLSM (Zeiss, Germany) and processed with the same setting for different treatments.

2.5. Quantitative real-time PCR (qRT-PCR)

Cell and tissue samples were collected for RNA extraction by using RNAiso Plus Reagent (Takara, Japan). The mRNA was transcribed into complementary DNA (cDNA) using the HiScript II Q RT SuperMix for qPCR Kit (Takara, Japan). qRT-PCR was performed using the ABI Prism 7500 PCR System (Applied Biosystems) at 95 °C for 10 min, followed by 40 cycles of 95 °C for 15 s and 60 °C for 60 s with SYBR Green (Takara, Japan). Primer sequences are listed in Table 1. Melt-curve analysis was used to verify the primer sets. Relative mRNA expression levels of specific genes were quantified using the $2^{-\Delta\Delta Ct}$ method values to that of *Gapdh*.

Table 1
The primers used in this study.

Genes	Sequence 5′ to 3′
Gapdh	Forward- AGAGTGTTTCCTCGTCCCG
	Reverse- CCGTTGAATTTGCCGTGA
Pparγ	Forward- GACCACTCGCATTCCTTT
	Reverse- ACAGACTCGGCACTCAAT
Pgc-1α	Forward- AGAAGCGGGAGTCTGAAA
	Reverse- CAGGTGTAACGGTAGGTG
Prdm16	Forward- GCGGTCAGCAATAGCAGC
	Reverse- CCCGTGGTAGTGTCCAAGTC
Ucp1	Forward- GCTTAATGACTGGAGGTGTG
	Reverse- GCTTTCTGTGGTGGCTAT
Dio2	Forward- AATTATGCCTCGGAGAAGACCG
	Reverse- GGCAGTTGCCTAGTGAAAGGT
Tbx1	Forward- ACCGAGATGATCGTCACCAAG
	Reverse- ACCAGCCAGGAGGAGCTATG
Tmem26	Forward- GACTCCACCAAACACTCC
	Reverse- GCATACTCCACGTCCACA
CytC	Forward- ATCTCCACGGTCTGTTCG
	Reverse- GCCCTTTCTCCCTTCTTC
Cox7a	Forward- GGCTCTGGTCCGGTCTT
	Reverse- CTGGGAGGTCATTGTCG
Cox8b	Forward- TGCGAAGTTCACAGTGGTT
	Reverse- GGCGGAAGTGGGAGTTTT
Aco2	Forward- ATCGAGCGGGGAAAGACATAC
	Reverse- TGATGGTACAGCCACCTTAGG
Uqcrc2	Forward- AAAGTTGCCCCGAAGGTTAAA
	Reverse- GAGCATAGTTTTCCAGAGAAGCA
mtTF	Forward- CCTCGTCTATCAGTCTTGT
	Reverse- GCTTCTGGTAGCTCCCTC
Hsl	Forward- AGCACTACAAACGCAACGA
	Reverse- CGACAGCACCTCAATCTCA
Cpt1	Forward- CGTGACGTTGGACGAATC
	Reverse- TCTGCGTTTATGCCTATC
Pparγ-promoter9	Forward- CCCTAGTCCTATCATTGATTCA
	Reverse- CGACCACTTTCATGGCTTA
Pgc-1α-promoter1	Forward- GCTGCCGGAGTCAGGACGA
	Reverse- GAAGGGAATGGCCGAGGG
Ucp1-promoter1	Forward- GGGCAATCTGGGCTTAAC
	Reverse- GCGTGAGTGCAAGAACAA
Ucp1-promoter	Forward- AGCTTGCTGTCACTCCTCTACA
	Reverse- TGAGGAAAGGGTTGACCTTG
Cox2 (mtDNA)	Forward- ATAACCGAGTCGTTCTGCCAAT
	Reverse- TTTCAGAGCATTGGCCATAGAA
Rsp18 (Genomic DNA)	Forward- CATCACCCACTTACCCCCAAAA
	Reverse- TGTGTTAGGGGACTGGTGGACA
C/ebpα	Forward- TCGGTGCGTCTAAGATGAGG
	Reverse- TGAGTATCCAAGGCACAAGGT
ap2	Forward- CCTTTGTGGGAACCTGGAA
	Reverse- TGTCGTCTGCGGTGATTT
Fas	Forward- GGGTCTATGCCACGATTC
	Reverse- GTGTCCCATGTTGGATTTG
Lpl	Forward- GAGGATGGCAAGCAACAC
	Reverse- AGCAGTTCTCCGATGTCC
Cidea	Forward- CTTCCTCGGCTGTCTCAA
	Reverse- TGGCTGCTCTTCTGTATCG
C/ebpβ	Forward- TGTCCACGTCGTCGTCGTCC
	Reverse- CCGTCAGCTCCAGCACCTTGT
Il-6	Forward- CACGGCCTTCCCTACTTC
	Reverse- TTTCCACGATTTCCCAGA

2.6. Western blotting

Cell and tissue samples were lysed in a RIPA lysis buffer containing phosphatase inhibitors and a protease inhibitor cocktail (Roche, USA). The lysates were centrifuged at 12,000 × *g* for 15 min at 4 °C, and the supernatants were collected. The protein samples were subjected to SDS-PAGE, transferred to polyvinylidene fluoride (PVDF) membranes, and sealed with 5% nonfat milk in TBS including 0.05% Tween-20 for 1 h at RT. Subsequently, the membranes were incubated overnight at 4 °C with specific primary antibodies, followed by incubating with appropriate HRP-conjugated secondary antibodies. The protein bands were visualized via chemiluminescence using an ECL kit (Beyotime, China). The primary antibodies used are as follows: GAPDH (AB0038, Abways, China), β-actin (P60709, Abways, China), PPARγ (sc-7273, Santa Cruz), PGC-1α (sc-13067, Santa Cruz), UCP1 (ab15517, Abcam), STAT3 (#4904, Cell Signaling), p-STAT3^{Tyr705} (#9145, Cell Signaling), TBX1 (bs-21501R, Bioss), Akt (AP0098, Abclonal), p-Akt^{Ser473} (A11016, Abclonal), p-ACC (AA110, Beyotime, China), ACC (AF1867, Beyotime, China) and aP2 (sc-271529, Santa Cruz).

2.7. Chromatin-immunoprecipitation (ChIP) assay

To determine the interaction of p-STAT3 with the promoter regions of *Pparγ*, *Pgc-1α*, and *Ucp1*, CHIP assay was performed using a CHIP Assay Kit (Beyotime, #P2078). ISO and AS-induced beige adipocytes were treated with Vehicle, IL6, Nic, or Nic+IL6, for 6 days. After immunoprecipitation with the anti-p-STAT3 antibody (1 μg, Cell Signaling, #9145) at 4 °C overnight, DNA-protein complexes were collected and treated according to the instruction of the manufacturer. The extracted DNA was used to test the promoter regions of *Pparγ*, *Pgc-1α*, and *Ucp1* by qPCR, respectively. The primers for *Pparγ*-promoter9, *Pgc-1α*-promoter1, and *Ucp1*-promoter1 were listed in Table 1.

To examine the binding of PPARγ with the promoter of *Ucp1*, CHIP assay was performed using beige adipocytes treated with Vehicle, IL6, GW, or GW + IL6, as described. The primers for the PPARγ-interacted *Ucp1*-promoter were shown in Table 1.

2.8. Co-immunoprecipitation (Co-IP)

Co-IP was performed as previously described [26], with some minor modifications. White SVFs culturing in 100-mm culture dishes were incubated with AS and ISO in the absence or presence of IL-6 for 6 days. The cells were lysed and aliquots of the cell extracts were incubated with the anti-PPARγ antibody (1 μg) at 4 °C overnight. Samples were incubated with protein A/G plus agarose beads and the extracts were washed. The bound proteins were released and examined by western blotting with anti-PPARγ and anti-PGC-1α antibodies, respectively.

2.9. Dual luciferase reporter assay

The 2.8-kb *Ucp1* promoter was ligated to the pGL3-basic vector to obtain pGL3-Ucp1p. HEK293 cells were co-transfected with 400 ng/mL of pGL3-basic, pGL3-Ucp1p, or pGL3-control along with 20 ng/mL of pRL-TK, respectively. Two days later, the cells were treated with Vehicle, IL6, GW, or GW+IL6 for 4 days. Subsequently, the treated cells were washed and lysed in 100 μL of lysis buffer (Dual reporter assay system, Promega). The firefly luciferase activity was examined according to the protocols, and efficiency was normalized to renilla luciferase activity directed by a co-transfected control plasmid pRL-TK.

2.10. Scanning electron microscopy (SEM)

iWAT and iBAT samples were fixed with 2% glutaraldehyde, and post-fixed in 1% osmium tetroxide for 1 h, dehydrated in graded concentrations of ethanol and 100% acetone. The specimens were dried at the critical point. Subsequently, the specimens were stuck on a colloidal silver, and sputtered with gold by a MED 010 coater (Balzers) and analyzed with a scanning electron microscope (JEOL, Japan).

2.11. Transmission electron microscopy (TEM)

iWATs from WT and KO mice were collected and fixed with 2% glutaraldehyde for 2 h at 4 °C, and post-fixed in 1% buffered osmium tetroxide for 2 h at 4 °C. Subsequently, the cells were dehydrated in graded concentrations of ethanol and 100% acetone. Then, the cells were embedded in durcopan and polymerized at 60 °C for 48 h, and ultrathin sections (60 nm) were obtained using RMC-PTX PowerTome (Boeckeler Instruments, USA). These sections were collected on 300-mesh copper grids, counterstained with uranyl acetate and lead citrate, and analyzed using a transmission electron microscope (Hitachi TCM system, Japan).

2.12. Histology, hematoxylin and eosin (H&E) staining, and oil-red-O (ORO) staining

Adipose and liver tissues were fixed in 4% formaldehyde solution overnight and encased in paraffin. Paraffin samples were sectioned (5 μm) and stained with H&E for histochemical examination. For ORO staining, liver samples were frozen in liquid nitrogen and sectioned at 8 μm in thickness using a cryostat. The sections were stained with ORO solution for 10 min, and with hematoxylin for 1 min after washing with water.

2.13. Quantification of mtDNA copy number

Equal amounts of WT and KO iBAT and iWAT were used to extract total DNA after digestion with proteinase K, respectively. The isolated DNA was used to amplify mtDNA using primers for the mitochondrial cytochrome *c* oxidase subunit 2 (*Cox2*) gene, with the *Rsp18* nuclear gene as an internal control of genomic DNA.

2.14. Cold challenge

Cold challenge experiment was conducted by individually placing six 15-week-old WT and IL-6-KO mice for 24 h at a 5 °C room, respectively. Core body temperature was monitored using a rectal probe every 3 or 6 h for the duration of the study (24 h). Finally, iWAT was collected to determine the mRNA expression of thermogenic-related genes and make sections.

2.15. Blood sample assay

Whole blood was collected from eyeball into heparinized containers and plasma was obtained by centrifugation at 1000 ×*g* for 10 min. Fasting glucose levels were determined by commercial kits (Njjc Bio Institute, China). Plasma insulin levels were detected by a commercial ELISA kit (Mlbio, China).

2.16. Glucose tolerance test (GTT) and insulin tolerance test (ITT)

For GTT, 15-week-old mice were fasted for 12 h prior to oral administration of glucose (2 g/kg body weight). Tail vein blood was obtained and glucose was determined using a commercial monitoring meter (Yuyue, China) at 0, 15, 30, 60, 90 and 120 min post glucose administration. For ITT, food was withdrawn 4 h before the test, and mice were injected intraperitoneally with insulin (0.75 U/kg body weight). Tail vein blood was collected and glucose was determined using a commercial monitoring meter at indicated time intervals.

2.17. Hepatic triglyceride (TG) and total cholesterol (TCH) content determination

Liver tissue (500 mg) was homogenized in 300 μL RIPA lysis buffer in a Polytron disrupter. The homogenate was centrifuged at 12,000*g* for 5 min, and the supernatant was collected. TG and TCH content in the tissue were quantified with commercial assay kits (Dongou, China), which was normalized to total protein and expressed as mmol/g total protein.

2.18. Statistical analysis

Statistical analysis was performed on data from at least 3 repeated experiments. Data were expressed as means ± SEM. Differences among multiple treatments were tested by one-way ANOVA, and differences between two groups were analyzed by student's *t*-test, using the SPSS statistics 22.0. Significance was established for $p < 0.05$ (*) and $p < 0.01$ (**).

3. Results

3.1. White adipocytes derived from IL-6-KO mice show lower beiging capability in vitro

In vitro experiment was performed to compare the thermogenic gene expression levels between WT- and IL-6-KO-derived adipocytes. We used ISO to induce beiging of in vitro cultured white adipocytes, and identified that both the mitochondria density and the UCP1 immunoreactivity were reduced in KO beiged adipocytes, compared to WT (Fig. 1A and B). Moreover, the mRNA levels of beiging-associated genes (*Pparγ*, *Pgc-1α*, *Ucp1*, *Dio2*, and *Tbx1*), and mitochondrial markers (*Cytc*, *Cox7a*, *Cox8b*, and *Aco2*) were all decreased in KO cells (Fig. 1C). Accordingly, IL-6-KO adipocytes possessed significantly lower PPARγ, PGC-1α, UCP1, and Tbx1 protein levels than did controls (Fig. 1D). These results demonstrate that IL-6-KO beiged adipocytes show lower mitochondria density and thermogenic gene expression in vitro, hinting an autocrine regulation of IL-6 on beiging of white adipocytes.

3.2. Exogenous IL-6 application enhances in vitro beiging of white adipocytes, partially via activating the phosphorylation of STAT3

To elucidate how IL-6 affects beiging of white adipocytes, exogenous IL-6 was supplemented into the beiging induction medium. It has been established that IL-6 can signal through the STAT3 signaling pathway [27]. We indeed observed a decrease of p-STAT3^{Tyr705}/STAT3 ratio in cultured IL-6-KO beiged adipocytes (Fig. 1D). Herein, four-day-induced WT beiging adipocytes were treated with exogenous IL-6 over a one-hour time course to further test the influence of IL-6 on STAT3 signaling. IL-6 did lead to an evident enhancement of STAT3^{Tyr705} phosphorylation, especially at the 15 min time point (Fig. 2A). To further determine whether STAT3 signaling was involved in IL-6 stimulation of white adipocyte beiging, a specific STAT3 inhibitor (Nic) was pre-added into the differentiation medium in the absence or presence of IL-6. Mitotracker and UCP1 immunofluorescence staining showed that

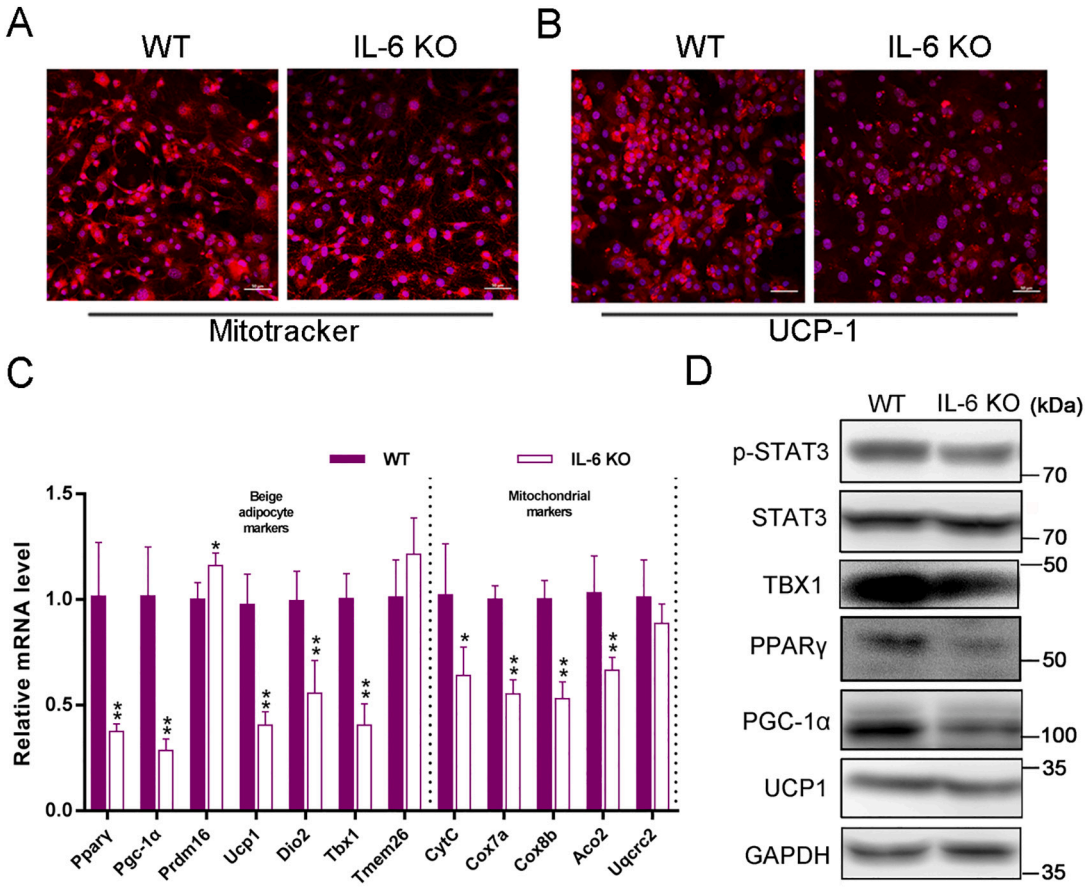

Fig. 1. White adipocytes derived from IL-6-KO mice show lower beiging capability in vitro. (A and B) MitoTracker staining (red) (A) and immunofluorescence staining of UCP1 (red) (B) of beiging white adipocytes derived from WT and KO mice. The nuclei (blue) were stained with DAPI. (C) Relative mRNA expression of genes involved in beiging in differentiated WT and IL-6-KO white adipocytes, determined by qRT-PCR. Data represent means ± SEM ($n = 4$). *$p < 0.05$, **$p < 0.01$ vs. WT. (D) Western blot analysis of p-STAT3^{Tyr705}, STAT3, PPARγ, PGC-1α, UCP1, and TBX1 protein contents in beiging white adipocytes derived from WT and KO mice. GAPDH serves as a loading control.

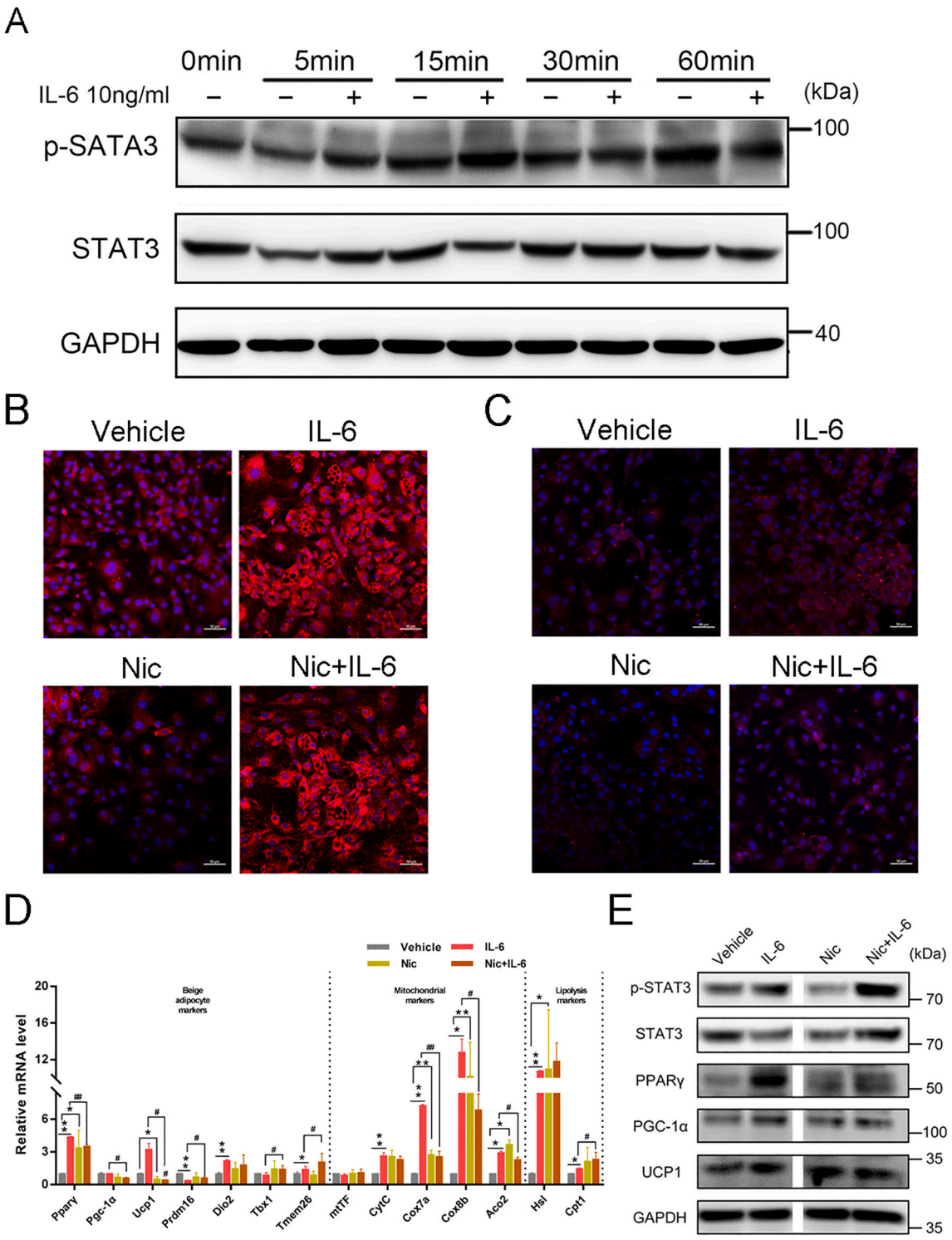

Fig. 2. Exogenous IL-6 application enhances beiging of white adipocytes partially via activating the phosphorylation of STAT3. (A) The protein expression profile of p-STAT3^{Tyr705} and STAT3 in beiging white adipocytes after supplementation with IL-6 or Vehicle for 5, 15, 30, and 60 min. GAPDH serves as an internal control. (B and C) MitoTracker staining (red) (B) and immunofluorescence staining of UCP1 (red) (C) of ISO-induced beiging white adipocytes upon treatments with Vehicle, IL-6, Nic (a specific stat3-inhibitor), or Nic+IL-6. Scale bar = 50 μm. The nuclei (blue) were stained with DAPI. (D) Relative mRNA expression levels of beiging-associated genes in treated cells, which was determined by qRT-PCR. Values represent average ± SEM ($n = 4$). $^{*}p < 0.05$, $^{**}p < 0.01$ compared with Vehicle; $^{\#}p < 0.05$, $^{\#\#}p < 0.01$ compared with IL-6 treatment. (E) Protein expression levels of p-STAT3^{Tyr705}, STAT3, PPARγ, PGC-1α, and UCP1 in cells treated with Vehicle, IL-6, Nic, or Nic+IL-6, which were determined by western blotting. GAPDH serves as an internal control.

exogenous IL-6 application evidently enhanced, while Nic suppressed, the mitochondria density and UCP1 expression (Fig. 2B and C). Moreover, the transcription stimulation of IL-6 on some beige adipocyte (*Pparγ*, *Pgc-1α*, and *Ucp1*) and mitochondrial (*Cox7a*, *Cox8b*, and *Aco2*) markers was substantially negated by Nic (Fig. 2D). Nic also blunted IL-6 enhancement on protein expression of PPARγ and PGC-1α (Fig. 2E). These data reveal that peripheral IL-6 activates white adipocyte beiging at least in part by stimulating STAT3 phosphorylation.

3.3. IL-6 induces the binding of p-STAT3^{Tyr705} to the promoter regions of *Pparγ* and *Ucp1*

Given that IL-6 activated STAT3 phosphorylation at Tyr705, and increased the transcription levels of *Pparγ*, *Pgc-1α*, and *Ucp1*, we speculated that p-STAT3^{Tyr705} might bind to specific promoter regions of these genes. By using ChIP assay, we surprisingly detected the association of p-STAT3 with the promoter regions of *Pparγ* and *Ucp1*, but not with that of *Pgc-1α* (Fig. 3A). Importantly, IL-6 application increased, whereas Nic decreased, the p-STAT3-interacted levels of *Pparγ* promoter (Fig. 3B). Similarly, IL-6 enhanced the association of p-STAT3 with *Ucp1* DNA, while Nic negated that interaction (Fig. 3C). These findings indicate that the IL-6-induced *Pparγ* and *Ucp1* expression was at least partially attributable to the transcriptional activation function of p-STAT3^{Tyr705}.

3.4. Enhanced PPARγ and PGC-1α interaction also contributes to IL-6 induction of UCP1 expression in beiging of white adipocytes

PPARγ is not only critical for adipogenesis, but also is essential for thermogenic gene expression by interacting with PGC-1α and/or PRDM16 [26,28,29]. To evaluate the importance of PPARγ, we detected the influence of GW (a specific PPARγ antagonist) on IL-6 stimulation of white adipocyte beiging. Surprisingly, GW indeed negated the induction of IL-6 on mitochondria density and UCP1 immuno-reactivity (Fig. 4A and B). GW also effectively suppressed IL-6 stimulation on the mRNA expression of several beiging- and mitochondria-associated genes, such as *Pparγ*, *Pgc-1α*, *Ucp1*, and *Cox8b* (Fig. 4C). Moreover, induction of IL-6 on protein contents of PPARγ, PGC-1α, and UCP1 was also decreased by GW (Fig. 4D).

Our results also showed the correlation of PGC-1α with the positive regulation of IL-6 on beiging of white adipocytes. Notably, the interaction degree of PGC-1α with PPARγ was increased by IL-6 application (Fig. 4E), which suggested the participation of PGC-1α in IL-6 stimulation of thermogenic gene expression. The expression level of UCP1, a downstream target of PPARγ/PGC-1α, determines the thermogenic capability for beige adipocytes [8,11]. Therefore, we further examined whether IL-6 interfered with interactions between PPARγ and the *Ucp1* promoter region. Results of ChIP assay indicated that PPARγ interaction with the *Ucp1* promoter was significantly increased in the presence of IL-6, but largely negated by GW treatment (Fig. 4F). Luciferase reporter activity driven by the *Ucp1* promoter showed that GW reduced *Ucp1* promoter-initiated luciferase activity that was induced by IL-6 (Fig. 4G). These results give evidence that the positive regulation of IL-6 on UCP1 expression also depends partially on the interaction of PGC-1α with PPARγ.

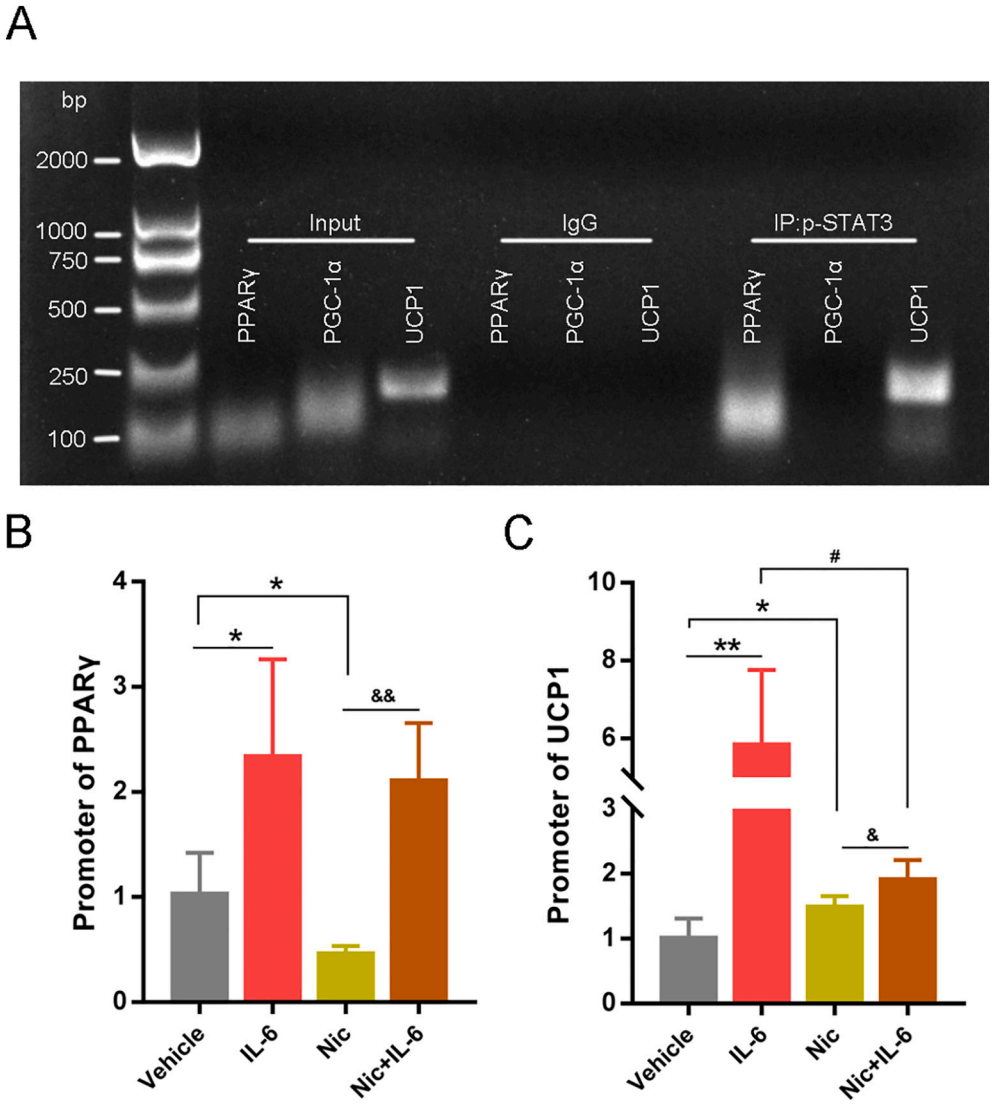

Fig. 3. IL-6 induces the binding of p-STAT3^{Tyr705} to the promoter regions of *Pparγ* and *Ucp1*. (A) ChIP analysis of p-STAT3 interaction with the promoter regions of *Pparγ*, *Pgc-1α,* and *Ucp1*. DNA was extracted from IL-6-treated beiging adipocytes, and immunoprecipitated with anti-p-STAT3-^{Tyr705} antibody or control IgG. (B) ChIP assay on the association of p-STAT3 with the *Pparγ* promoter in beiging adipocytes treated with Vehicle, IL-6, Nic, or Nic+IL-6 ($n = 4$). (C) ChIP assay on the interaction of p-STAT3 with the *Ucp1* promoter in beiging adipocytes treated with Vehicle, IL-6, Nic, or Nic+IL-6 ($n = 4$). $^{*}p < 0.05$, $^{**}p < 0.01$ compared with Vehicle; $^{\#}p < 0.05$ compared with IL-6 treatment; $^{\&}p < 0.05$, $^{\&\&}p < 0.01$ compared with Nic treatment.

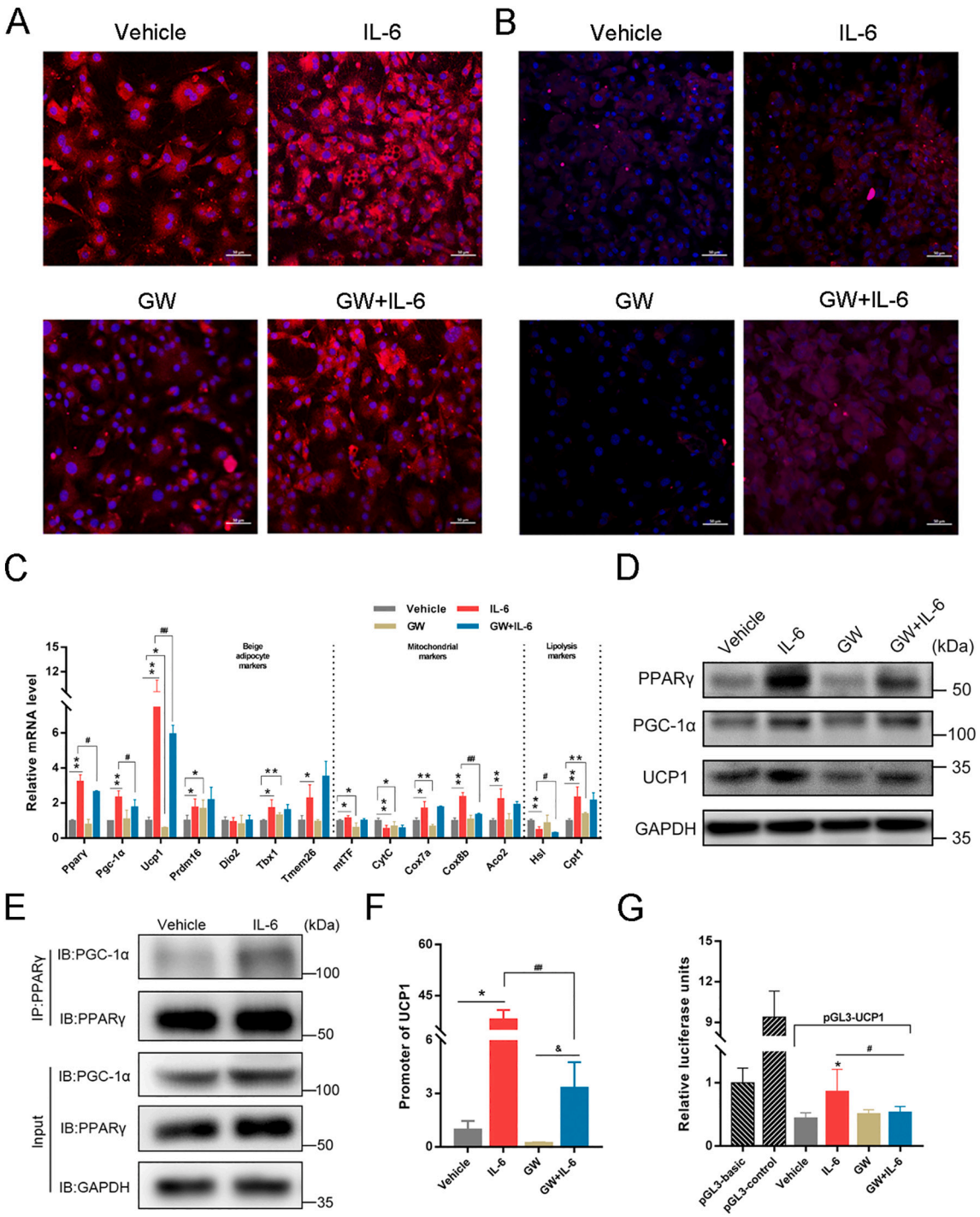

Fig. 4. PPARγ and PGC-1α participate in the regulation of IL-6 on beiging of white adipocytes. (A and B) Mitotracker staining (red) (A) and UCP1 immunostaining (red) (B) of ISO-induced beiging adipocytes upon treatments with Vehicle, IL-6, GW, or GW+IL-6. (C) Relative mRNA levels of beiging- and mitochondria-associated markers in cells treated as in (A), determined by qRT-PCR ($n = 4$). (D) Western blot analysis of the protein expression of PPARγ, PGC-1α, and UCP1 in cells treated as in (A). (E) Co-IP analysis of association of PGC-1α with PPARγ in ISO-induced beiging white adipocytes treated with Vehicle or IL-6. (F) ChIP assay on the interaction of PPARγ with the *Ucp1* promoter in beiging adipocytes treated with Vehicle, IL-6, GW, or GW+IL-6 ($n = 4$). (G) Luciferase activity determination of UCP1 translation in HEK293 cells treated with Vehicle, IL-6, GW, or GW+IL-6 ($n = 5$). $^{*}p < 0.05$, $^{**}p < 0.01$ vs. Vehicle; $^{\#}p < 0.05$, $^{\#\#}p < 0.01$ vs. IL-6 treatment.

3.5. IL-6 gene disruption is associated with decreased beiging of white fat and STAT3 tyrosine phosphorylation

24-week-old male WT and IL-6-KO mice were employed to further evaluate the role of IL-6 in the thermogenic potential of adipose tissues. Though the final body weight of IL-6 KO mice was significantly lower than that of WT animals, the food efficiency did not differ between the two littermates (Fig. 5A–C). Notably, IL-6 KO mice had markedly more subcutaneous fat than the WT, but the iBAT appearance was indistinguishable between the two phenotypes (Supplementary Fig. 1). Compared with WT animals, the iWAT index in IL-6-KO mice was slightly but not significantly increased (Fig. 5D), which could be intuitively discovered from the representative graphs of iWAT (Fig. 5E).

SEM and H&E staining pictures showed larger adipocyte size in KO

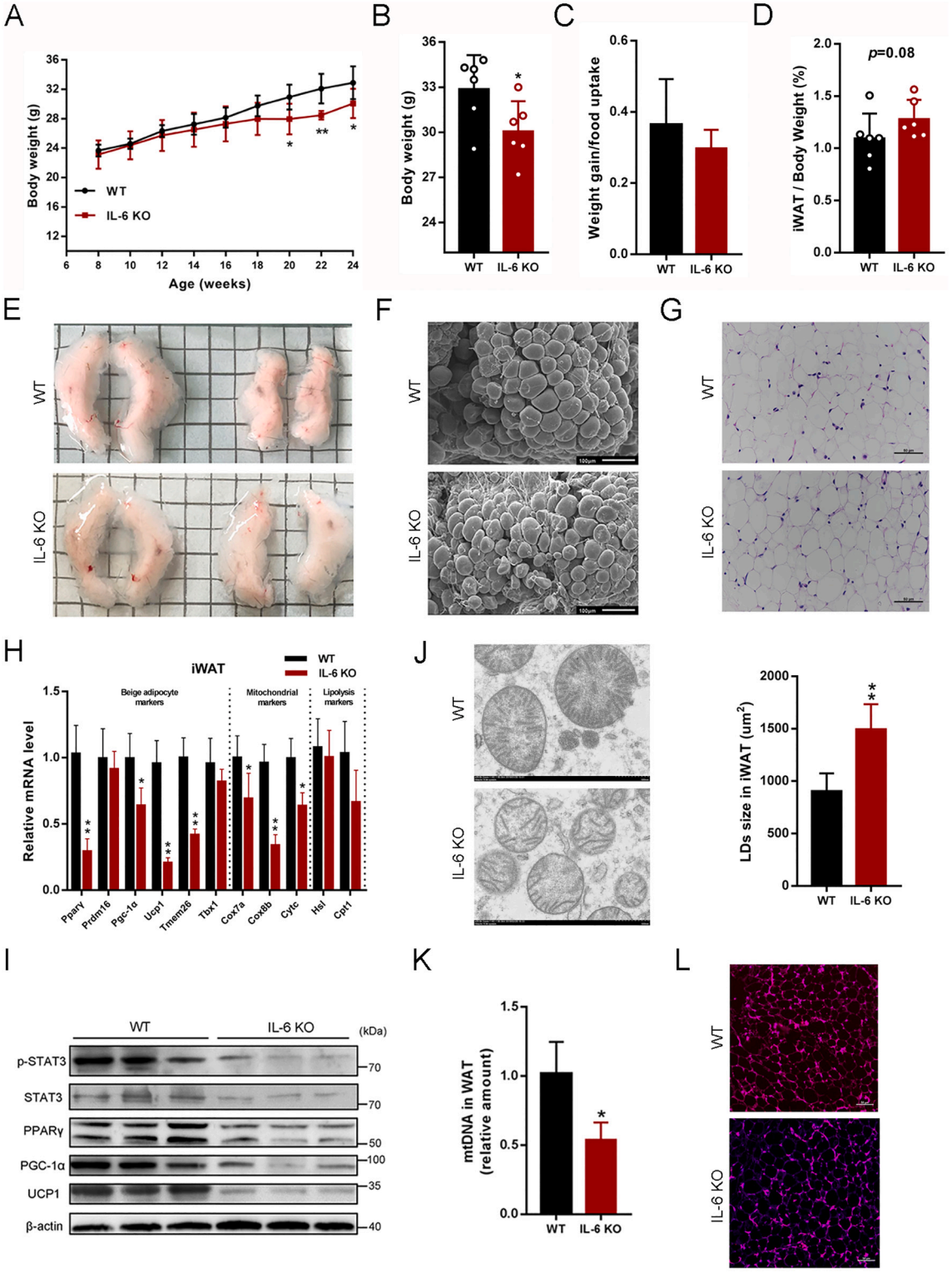

Fig. 5. IL-6 gene disruption is associated with decreased beiging of white fat and STAT3 tyrosine phosphorylation. Tissue samples were from 24-week-old WT and IL-6-KO mice. (A) Dynamic changes in body weight of male WT and IL-6-KO mice from 3- to 24-week-old ($n = 6$). (B) Body weight of 24-week-old WT and IL-6-KO mice ($n = 6$). (C) The whole body weight gain/feed intake ratio of WT and IL-6-KO mice for 21 weeks. (D and E) The iWAT/body weight ratios (D) and representative iWAT images (E) of WT and IL-6-KO mice ($n = 6$). (F) Representative SEM images of iWAT tissue sections. Scale bar = 100 μm. (G) Representative H&E-stained images of iWAT tissue sections, and the lipid droplet sizes in iWAT. Scale bar = 50 μm. (H) The relative mRNA levels of beige adipocyte-, mitochondria-, and lipolysis-associated markers in iWAT of WT and IL-6-KO mice, determined by qRT-PCR (n = 6). (I) Western blot analysis of the protein contents of p-STAT3^{Tyr705}, STAT3, PPARγ, PGC-1α and UCP1 in iWAT of WT and IL-6-KO mice. Blots were stripped and reprobed β-actin to normalize for variation in loading and transfer of proteins. (J) Representative TEM images of mitochondria in WT and IL-6-KO iWAT. Scale bar = 500 nm. (K) The relative mtDNA amount in iWAT of WT and IL-6-KO mice ($n = 6$). (L) Immunofluorescence staining of UCP1 in WT and IL-6-KO iWAT. Scale bar = 50 μm. *$p < 0.05$, **$p < 0.01$ compared with WT samples.

iWAT vs. that of WT (Fig. 5F and G), which was a characteristic of accelerated triglyceride accumulation or reduced triglyceride liberation. Strikingly, some adipogenic differentiation general genes, including *C/ebpα*, *ap2*, and *Lpl*, as well as aP2 protein were up-regulated in KO iWAT (Supplementary Fig. 2), indicating the increased adipocyte size was partially due to triglyceride accumulation induction. In addition, the transcription of some beige adipocyte markers (*Tmem26*, *Pparγ*, *Pgc-1α*, and *Ucp1*), and essential factors involved in mitochondria function (*Cox7a*, *Cox8b*, and *Cytc*) was significantly reduced in KO iWAT (Fig. 5H). Likewise, IL-6-KO iWAT also showed decreased protein levels of PPARγ, PGC-1α and UCP1 (Fig. 5I). Moreover, TEM photos indicated that the mitochondrion size in KO iWAT was markedly decreased (Fig. 5J). Also, less mitochondria copy number (Fig. 5K) and lower intense UCP1 immuno-reactivity (Fig. 5L) were visible in KO iWAT. Notably, IL-6 KO inhibited phosphorylation of STAT3 at Tyr705 (Fig. 5I). These findings suggest that IL-6 gene deletion leads to suppressed beiging degree of white fat, associating with suppressed tyrosine phosphorylation of STAT3.

3.6. iWAT of IL-6-KO mice shows decreased response to cold challenge

Given the suppressed beiging capability of white fat due to IL-6 deficiency, we further tested its response to cold challenge. Strikingly, the rectal temperature of the two littermates was comparable at corresponding time points (Fig. 6A). H&E staining showed that cold challenge effectively increased the number of multilocular adipocytes in both WT and KO iWAT (Fig. 6B). However, KO iWAT owned less activation of UCP1 expression than the WT (Fig. 6D). Additionally, following cold challenge, iWAT of KO mice displayed lower increase of beige adipocyte markers (*Pparγ*, *Dio2*, *Tbx1*, *Tmem26*, and *Ucp1*), mitochondrial markers (*CytC*, *Cox7a*, *Cox8b*, and *Uqcrc2*), as well as lipolysis markers (*Hsl* and *Cpt1*) (Fig. 6C). These data demonstrate that KO iWAT shows lower cold-response than the WT iWAT.

3.7. IL-6 gene deletion disrupts glucose homeostasis

In view of the blockade of IL-6 KO on beiging of white fat, its impact on glucose metabolism-related parameters was determined. Interestingly, the plasma glucose level of KO mice was substantially increased ($p < 0.05$), but the insulin content was not significantly changed (Fig. 7A and C). Thus, GTT and ITT were performed. GTT indicated that IL-6 KO mice showed significantly decreased glucose tolerance compared to WT mice (Fig. 7B). ITT further gave evidence that IL-6-KO mice were less insulin-sensitive than control animals, though not significantly (Fig. 7D). Consistent with the decreased glucose and insulin response, the activation of insulin on Akt phosphorylation in iWAT and muscle was reduced in IL-6-KO mice (Fig. 7E and F). Thus, the increased basal glucose level and decreased glucose tolerance are likely due to the reduced insulin sensitivity in KO mice.

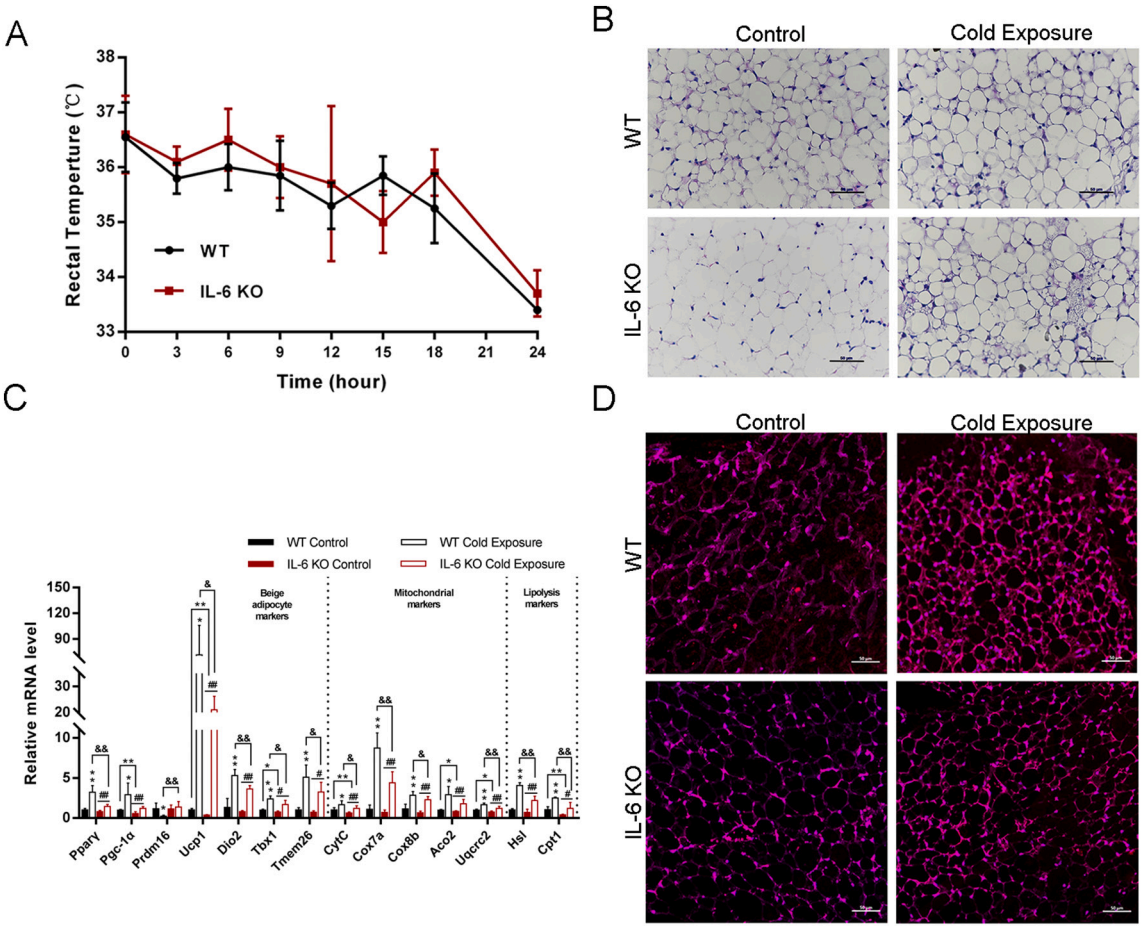

Fig. 6. IL-6-KO iWAT shows lower response to cold challenge. (A) Core body temperature in 15-week-old WT and IL-6-KO mice monitored using a rectal probe every 3 or 6 h for a 24-h cold challenge duration ($n = 5$). (B and D) Representative images of H&E staining (B) and immunofluorescence staining of UCP1 (C) of iWAT sections, under normal temperature or cold challenge for 24 h. Scale bar = 50 μm. (C) qRT-PCR analysis of beige adipocyte-, mitochondria-, and lipolysis-related gene expression in WT and IL-6^{-}KO iWAT under normal temperature or cold challenge for 24 h. Values represent average ± SEM ($n = 6$). $^{*}p < 0.05$, $^{**}p < 0.01$ compared with WT in the normal temperature; $^{\#}p < 0.05$, $^{\#\#}p < 0.01$ compared with IL-6-KO mice in the normal temperature; $^{\&}p < 0.05$, $^{\&\&}p < 0.01$ compared with WT mice upon cold challenge.

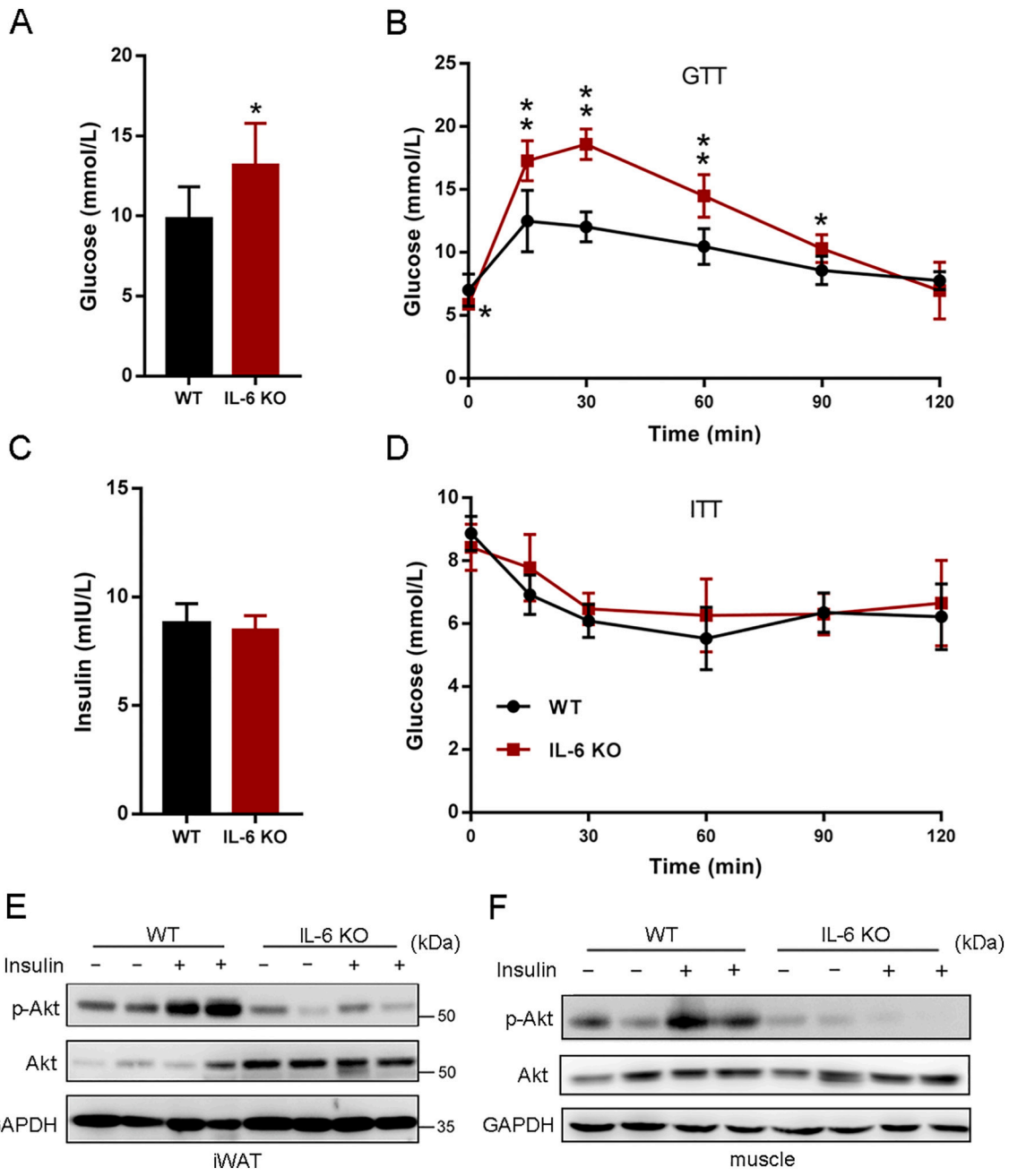

Fig. 7. IL-6 gene deletion disrupts glucose homeostasis in mature mice. (A and B) Plasma glucose (A) and insulin (B) levels in WT and IL-6-KO mice after fasting for 12 h ($n = 6$). (C) Glucose tolerance tests (GTT) in 15-week-old WT and IL-6-KO mice after fasting for 16 h ($n = 5$). (D) Insulin tolerance tests (ITT) in 15-week-old WT and IL-6-KO mice after fasting for 4 h ($n = 5$). (E and F) Western blot analysis of the protein contents of p-Akt and Akt in iWAT (E) and muscle (F) of WT and IL-6-KO mice, following Vehicle or insulin treatment. Values represent average ± SEM. $^{*}p < 0.05$, $^{**}p < 0.01$ compared with WT samples.

3.8. IL-6 gene deletion mice develop severer hepatic steatosis

The effect of IL-6 gene deletion on hepatic fat deposition was next investigated. Interestingly, compared with WT, IL-6-KO mice appeared to have relative larger livers under chow diet, as revealed by gross morphology and the liver index (Fig. 8A and B). Even under chow diet feeding conditions, the liver sections of KO mice had more fat accumulation and ORO-stained lipid droplets (Fig. 8C). Similarly, the hepatic levels of TG and TCH were elevated by IL-6 gene deletion (Fig. 8D and E).

Subsequently, we determined the influence of IL-6 disruption on hepatic steatosis upon 21 weeks' HFD feeding. The livers of HFD-fed IL-6 KO mice were visibly larger and the liver index was significantly higher than WT (Fig. 8F and G). H&E and ORO staining of liver sections (Fig. 8H), as well as the elevated hepatic TG and TCH contents (Fig. 8Iand J) gave further evidences for the acceleration of IL-6 disruption on HFD-induced hepatic steatosis. These results suggest that IL-6 gene deletion accelerated the progression of hepatic steatosis. Furthermore, the transcriptional levels of *Pparγ*, *Pgc-1α*, *Ucp1*, *Cidea*, *Prdm16*, and *C/ebpβ* were all significantly down-regulated in HFD-fed KO iWAT (Supplementary Fig. 3), which suggested that the hepatic steatosis phenotype associated with IL-6 deficiency is due in large measure to the decreased thermogenic capability of beige fats.

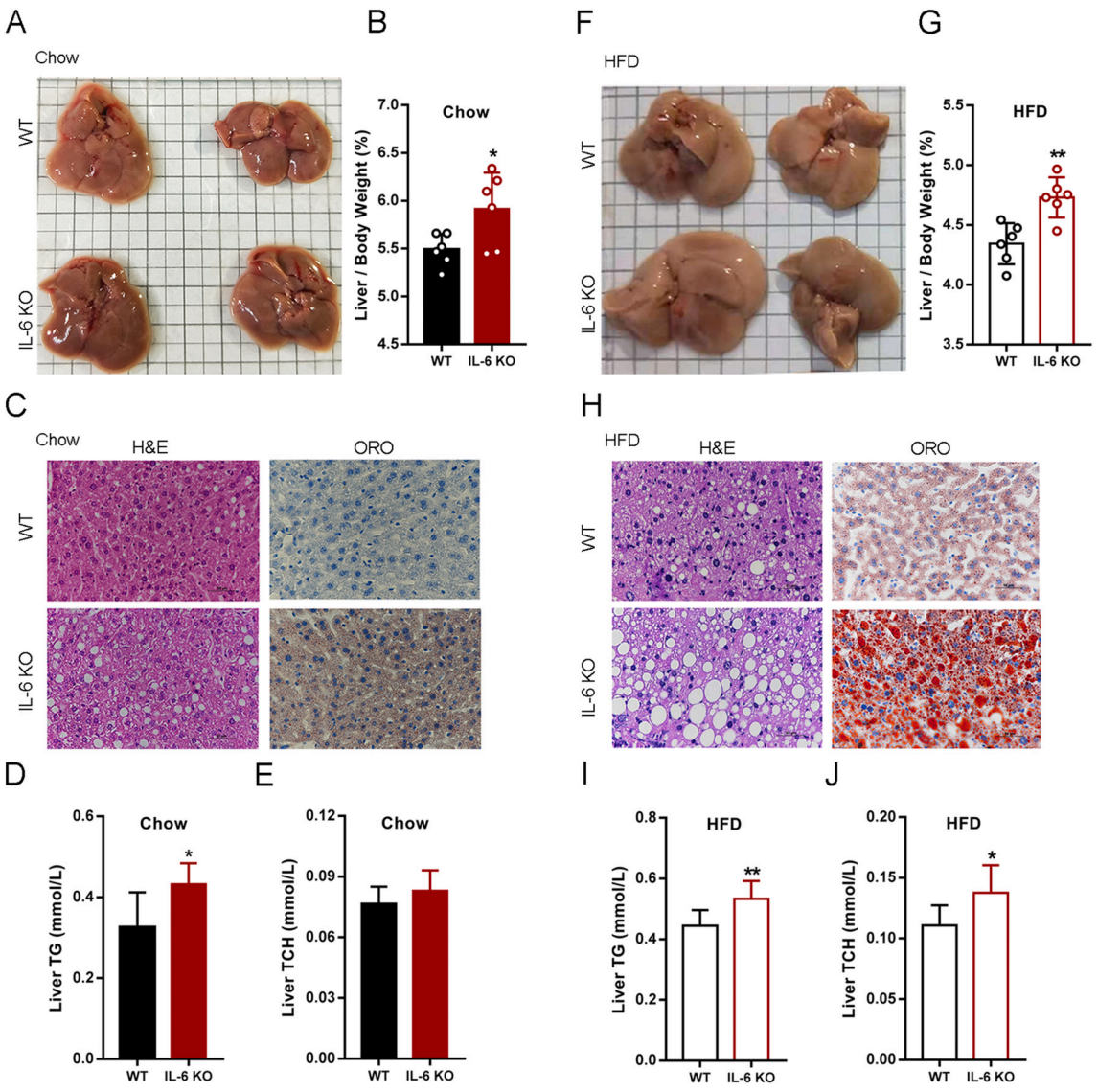

Fig. 8. IL-6 gene deletion increases hepatic fat deposition under both chow and HFD fed conditions. (A) Representative liver images from WT and IL-6-KO mice (chow diet). (B) The ratios of liver/body weight of WT and IL-6-KO mice (chow diet). (C) H&E staining and ORO staining of liver sections from WT and IL-6-KO mice (chow diet). (D and E) TG (D) and TCH (E) contents in the livers of WT and IL-6-KO mice (chow diet). (F) Representative liver images from WT and IL-6-KO mice (HFD). (G) The ratios of liver/body weight of WT and IL-6-KO mice (HFD). (H) H&E staining and ORO staining of liver sections from WT and IL-6-KO mice (HFD). (I and J) TG (I) and TCH (J) contents in the livers of WT and IL-6-KO mice (HFD). Data represent means ± SEM ($n = 6$). *$p < 0.05$, **$p < 0.01$ vs. WT samples.

4. Discussion

Apart from cells of the immune system [23], IL-6 is expressed in adipose tissue [4], skeletal muscle [30], as well as centrally in hypothalamic nuclei [31] and lateral parabrachial nucleus [25]. IL-6 has emerged as a highly versatile cytokine with important repercussions for the endocrine system, particularly in obesity and insulin resistance [18,19,32]. In the present study, we firstly demonstrated the positive regulation of peripheral IL-6 signaling in beiging of white fat, which are evidenced by the exogenous IL-6 stimulation and the IL-6 KO inhibition on the beiging degree of white adipocytes. In addition, the elevation of thermogenic gene expression by endogenous IL-6 (Supplementary Fig. 4) further indicated that IL-6 takes action via a cell-autonomous manner. Different from previous reports on the central regulation of IL-6 in thermogenic gene expression of brown fat [24,25], our study uncovers a novel effect of peripheral IL-6 on beiging of white fat.

Furthermore, we elucidated that the STAT3 signaling is at least partially involved in the IL-6 activation of white fat beiging process. It has been established that the phosphorylated STAT3 can be dimerized and translocated to the nucleus, which binds to consensus response elements in the promoters of target genes, thus inducing the transcription of these genes [16,27]. In the present study, we found the correlation of p-STAT3^{Tyr705} with *Pparγ*, *Pgc-1α*, and *Ucp1* expression. Surprisingly, we determined the interaction of p-STAT3^{Tyr705} with the promoter regions of *Pparγ* and *Ucp1*. To the best of our knowledge, this is the first report of p-STAT3^{Tyr705} taking action as a transcriptional factor to induce the transcription of *Pparγ* and *Ucp1*, suggesting another function of p-STAT3^{Tyr705}. At the moment, it is not clear how *Pgc-1α* expression is induced following IL-6 application. However, it can be concluded that the elevated PGC-1α protein content is contributing to mitochondrial marker genes expression, as well as PGC-1α-PPARγ interaction [33]. Collectively, our data demonstrated the importance of p-STAT3^{Tyr705}-induced *Pparγ* and *Ucp1* transcription, and PGC-1α-PPARγ protein interaction in the regulation of IL-6 on white adipocyte beiging.

Subsequently, we determined that IL-6-KO mice showed lower beiging degree of white fat, but did not with alteration in the

thermogenic capability of BAT under basal conditions (Supplementary Fig. 5). Consistently, iWAT in IL-6-KO mice showed decreased response to cold challenge. The comparable rectal temperature changes of WT and KO mice following cold challenge may be attributable to the unaltered thermogenic capability of BAT. This seems to be inconsistent with previous studies, of which indicated that central *Il-6* gene delivery [24] or microinjection [25] increases the expression of UCP1 in BAT. We speculated that global IL-6 KO is not sufficient to change the thermogenic potential of BAT under basal conditions, but central IL-6 elevation is able to do so. Furthermore, under HFD-fed condition, the thermogenic gene expression in KO iWAT was also decreased, which was associated with the development of severe hepatic steatosis. These findings suggested that the hepatic steatosis phenotype associated with IL-6 deficiency observed in the present and previous studies [22] is due in part to the decreased thermogenic capability of beige fats.

Moreover, accompanied with the decreased white fat beiging degree in IL-6-KO mice, glucose homeostasis was disrupted as well. This result is consistent with several previous reports. Mauer et al. [32] indicated that myeloid cell IL-6Rα disruption leads to insulin resistance and deteriorated glucose homeostasis during diet-induced obesity. Timper et al. [34] found central application of IL-6 improves glucose homeostasis in obesity via the trans-signaling pathway. In contrast, there are some opposite findings on the role of IL-6 signaling in glucose homeostasis. For example, conditional inactivation of IL-6Ra in natural killer cells was demonstrated to protect mice from insulin resistance [35]. Xu et al. [23] evidenced that T lymphocyte-specific deletion of *IL-6Rα* improves glucose tolerance and insulin sensitivity early during obesity development. It can be seen that the influence of IL-6 signaling on insulin sensitivity and glucose homeostasis is dependent on how and where the signaling are changed. The disrupted glucose homeostasis observed in our KO mice may be due largely to the blunted thermogenic ability of beige adipocytes, as enhanced beiging degree often associates with higher insulin sensitivity [36].

Taken together, we describe a novel peripheral regulation of IL-6 signaling on white fat beiging. IL-6 positively correlates with thermogenic gene expression in beige adipocytes, which is dependent on the STAT3 signaling. IL-6 KO predisposes mice to lower thermogenic potential of beige fat, disrupted glucose homeostasis and severer hepatic steatosis. These findings give evidences that peripheral IL-6 is essential for white fat beiging, which hint enhancing IL-6/STAT3 signaling would be considered to combat obesity and associated disorders. Future in vivo studies will further detect the contribution of peripheral IL-6/STAT3 to the stimulation of white fat beiging.

CRediT authorship contribution statement

Haifang Li and Mei Dong performed in vivo experiments, wrote the manuscript, organized the literature and figures. Wenhui Liu conducted in vitro experiments and performed statistical analysis. Haifang Li, Qingxin Liu and Hai Lin conceived the project, led and supervised the study, and reviewed/edited the manuscript. Cheng Gao, Yanxin Jia, Xinzhi Zhang, and Xue Xiao performed experiments and contributed to discussion.

Declaration of competing interest

The authors declare that they do not have any conflict of interest.

Acknowledgments

The authors would like to thank Zizhang Zhou (Shandong Agricultural University) and Shuxin Zhang (Shandong Agricultural University) for their assistance in ChIP assay. This work was supported by the National Key Research and Development Program of China (No. 2017YFE0129800), the Taishan Scholars Program [No. 201511023, 201712022], Funds of Shandong "Double Tops" Program, and Natural Science Foundation of Shandong Province, China [No. ZR2019MC016].

Appendix A. Supplementary data

Supplementary data to this article can be found online at https://doi.org/10.1016/j.bbamcr.2021.119080.

References

[1] E.D. Rosen, B.M. Spiegelman, What we talk about when we talk about fat, Cell 156 (1–2) (2014) 20–44, https://doi.org/10.1016/j.cell.2013.12.012.
[2] G. Karsenty, Convergence between bone and energy homeostases: leptin regulation of bone mass, Cell Metab. 4 (5) (2006) 341–348, https://doi.org/10.1016/j.cmet.2006.10.008.
[3] N. Kubota, W. Yano, T. Kubota, T. Yamauchi, S. Itoh, H. Kumagai, et al., Adiponectin stimulates AMP-activated protein kinase in the hypothalamus and increases food intake, Cell Metab. 6 (1) (2007) 55–68, https://doi.org/10.1016/j.cmet.2007.06.003.
[4] V. Mohamed-Ali, S. Goodrick, A. Rawesh, D.R. Katz, J.M. Miles, J.S. Yudkin, et al., Subcutaneous adipose tissue releases interleukin-6, but not tumor necrosis factor-alpha, in vivo, Clin. Endocrinol. Metab. 82 (12) (1997) 4196–4200, https://doi.org/10.1210/jcem.82.12.4450.
[5] L. Poekes, N. Lanthier, I.A. Leclercq, Brown adipose tissue: a potential target in the fight against obesity and the metabolic syndrome, Clin. Sci. (Lond.) 129 (11) (2015) 933–949, https://doi.org/10.1042/CS20150339.
[6] A. Bartelt, J. Heeren, Adipose tissue browning and metabolic health, Nat. Rev. Endocrinol. 10 (1) (2014) 24–36, https://doi.org/10.1038/nrendo.2013.204.
[7] N.H. Rogers, Brown adipose tissue during puberty and with aging, Ann. Med. 47 (2) (2015) 142–149, https://doi.org/10.3109/07853890.2014.914807.
[8] J. Wu, P. Boström, L.M. Sparks, L. Ye, J.H. Choi, A.H. Giang, et al., Beige adipocytes are a distinct type of thermogenic fat cell in mouse and human, Cell 150 (2) (2012) 366–376, https://doi.org/10.1016/j.cell.2012.05.016.
[9] K.A. Virtanen, M.E. Lidell, J. Orava, M. Heglind, R. Westergren, T. Niemi, et al., Functional brown adipose tissue in healthy adults, N. Engl. J. Med. 360 (15) (2009) 1518–1525, https://doi.org/10.1056/NEJMoa0808949.
[10] M. Saito, Y. Okamatsu-Ogura, M. Matsushita, K. Watanabe, T. Yoneshiro, J. Nio-Kobayashi, et al., High incidence of metabolically active brown adipose tissue in healthy adult humans: effects of cold exposure and adiposity, Diabetes 58 (7) (2009) 1526–1531, https://doi.org/10.2337/db09-0530.
[11] S.Y. Min, J. Kady, M. Nam, R. Rojas-Rodriguez, A. Berkenwald, J.H. Kim, Human 'brite/beige' adipocytes develop from capillary networks, and their implantation improves metabolic homeostasis in mice, Nat. Med. 22 (3) (2016) 312–318, https://doi.org/10.1038/nm.4031.
[12] Hotamisligil GS (2008) Inflammation and endoplasmic reticulum stress in obesity and diabetes. Int. J. Obes. (Lond) 32 Suppl 7:S52-4. doi:https://doi.org/10.1038/ijo.2008.238.
[13] A.L. Carey, C.R. Bruce, M. Sacchetti, M.J. Anderson, D.B. Olsen, B. Saltin, et al., Interleukin-6 and tumor necrosis factor-alpha are not increased in patients with Type 2 diabetes: evidence that plasma interleukin-6 is related to fat mass and not insulin responsiveness, Diabetologia 47 (6) (2004) 1029–1037, https://doi.org/10.1007/s00125-004-1403-x.
[14] M. Lee, S.J. Song, M.S. Choi, R. Yu, T. Park, IL-7 receptor deletion ameliorates diet-induced obesity and insulin resistance in mice, Diabetologia 58 (10) (2015) 2361–2370, https://doi.org/10.1007/s00125-015-3684-7.
[15] I.T. Harley, T.E. Stankiewicz, D.A. Giles, S. Softic, L.M. Flick, M. Cappelletti, et al., IL-17 signaling accelerates the progression of nonalcoholic fatty liver disease in mice, Hepatology 59 (5) (2014) 1830–1839, https://doi.org/10.1002/hep.26746.
[16] P.C. Heinrich, I. Behrmann, S. Haan, H.M. Hermanns, G. Müller-Newen, F. Schaper, Principles of interleukin (IL)-6-type cytokine signalling and its regulation, Biochem. J. 374 (Pt 1) (2003) 1–20, https://doi.org/10.1042/BJ20030407.
[17] G. Van Hall, A. Steensberg, M. Sacchetti, C. Fischer, C. Keller, P. Schjerling, et al., Interleukin-6 stimulates lipolysis and fat oxidation in humans, J. Clin. Endocrinol. Metab. 88 (7) (2003) 3005–3010, https://doi.org/10.1210/jc.2002-021687.
[18] Wallenius K, Jansson JO, Wallenius V. The therapeutic potential of interleukin-6 in treating obesity. Expert Opin. Biol. Ther. 3(7):1061–70. doi:https://doi.org/10.1517/14712598.3.7.1061.
[19] K. Wallenius, V. Wallenius, D. Sunter, S.L. Dickson, J.O. Jansson, Intracerebroventricular interleukin-6 treatment decreases body fat in rats, Biochem. Biophys. Res. Commun. 293 (1) (2002) 560–565, https://doi.org/10.1016/S0006-291X(02)00230-9.
[20] Y. Ma, M. Gao, H. Sun, D. Liu, Interleukin-6 gene transfer reverses body weight gain and fatty liver in obese mice, Biochim. Biophys. Acta 1852 (5) (2015) 1001–1011, https://doi.org/10.1016/j.bbadis.2015.01.017.
[21] V. Wallenius, K. Wallenius, B. Ahrén, M. Rudling, H. Carlsten, S.L. Dickson, et al., Interleukin-6-deficient mice develop mature-onset obesity, Nat. Med. 8 (1) (2002) 75–79, https://doi.org/10.1038/nm0102-75.
[22] V.B. Matthews, T.L. Allen, S. Risis, M.H. Chan, D.C. Henstridge, N. Watson, et al., Interleukin-6-deficient mice develop hepatic inflammation and systemic insulin resistance, Diabetologia 53 (11) (2010) 2431–2441, https://doi.org/10.1007/s00125-010-1865-y.
[23] E. Xu, M. Pereira, I. Karakasilioti, S. Theurich, M. Al-Maarri, G. Rappl, et al., Temporal and tissue-specific requirements for T-lymphocyte IL-6 signalling in

obesity-associated inflammation and insulin resistance, Nat. Commun. 8 (2017) 14803, https://doi.org/10.1038/ncomms14803.
[24] G. Li, R.L. Klein, M. Matheny, M.A. King, E.M. Meyer, P.J. Scarpace, Induction of uncoupling protein 1 by central interleukin-6 gene delivery is dependent on sympathetic innervation of brown adipose tissue and underlies one mechanism of body weight reduction in rats, Neuroscience 115 (3) (2002) 879–889, https://doi.org/10.1016/s0306-4522(02)00447-5.
[25] D. Mishra, J.E. Richard, I. Maric, B. Porteiro, M. Häring, S. Kooijman, et al., Parabrachial interleukin-6 reduces body weight and food intake and increases thermogenesis to regulate energy metabolism, Cell Rep. 26 (11) (2019) 3011–3026, https://doi.org/10.1016/j.celrep.2019.02.044.
[26] P. Seale, H.M. Conroe, J. Estall, S. Kajimura, A. Frontini, J. Ishibashi, et al., Prdm16 determines the thermogenic program of subcutaneous white adipose tissue in mice, J. Clin. Invest. 121 (1) (2011) 96–105, https://doi.org/10.1172/JCI44271.
[27] Z. Zhong, Z. Wen, J.E. Darnell Jr., Stat3: a STAT family member activated by tyrosine phosphorylation in response to epidermal growth factor and interleukin-6, Science 264 (5155) (1994) 95–98, https://doi.org/10.1126/science.8140422.
[28] M. Ahmadian, J.M. Suh, N. Hah, C. Liddle, A.R. Atkins, M. Downes, et al., PPARγ signaling and metabolism: the good, the bad and the future, Nat. Med. 19 (5) (2013) 557–566, https://doi.org/10.1038/nm.3159.
[29] P. Puigserver, B.M. Spiegelman, Peroxisome proliferator-activated receptor-gamma coactivator 1 alpha (PGC-1 alpha): transcriptional coactivator and metabolic regulator, Endocr. Rev. 24 (1) (2003) 78–90, https://doi.org/10.1210/er.2002-0012.
[30] K. Ostrowski, T. Rohde, M. Zacho, S. Asp, B.K. Pedersen, Evidence that interleukin-6 is produced in human skeletal muscle during prolonged running, J. Physiol. 508 (Pt 3) (1998) 949–953, https://doi.org/10.1111/j.1469-7793.1998.949bp.x.
[31] K. Shizuya, T. Komori, R. Fujiwara, S. Miyahara, M. Ohmori, J. Nomura, The expressions of mRNAs for interleukin-6 (IL-6) and the IL-6 receptor (IL-6R) in the rat hypothalamus and midbrain during restraint stress, Life Sci. 62 (25) (1998) 2315–2320, https://doi.org/10.1016/s0024-3205(98)00212-4.
[32] J. Mauer, B. Chaurasia, J. Goldau, M.C. Vogt, J. Ruud, K.D. Nguyen, et al., Signaling by IL-6 promotes alternative activation of macrophages to limit endotoxemia and obesity-associated resistance to insulin, Nat. Immunol. 15 (5) (2014) 423–430, https://doi.org/10.1038/ni.2865.
[33] Z. Wu, P. Puigserver, U. Andersson, C. Zhang, G. Adelmant, V. Mootha, et al., Mechanisms controlling mitochondrial biogenesis and respiration through the thermogenic coactivator PGC-1, Cell 98 (1) (1999) 115–124, https://doi.org/10.1016/S0092-8674(00)80611-X.
[34] K. Timper, J.L. Denson, S.M. Steculorum, C. Heilinger, L. Engström-Ruud, C. M. Wunderlich, et al., IL-6 improves energy and glucose homeostasis in obesity via enhanced central IL-6 trans-signaling, Cell Rep. 19 (2) (2017) 267–280, https://doi.org/10.1016/j.celrep.2017.03.043.
[35] S. Theurich, E. Tsaousidou, R. Hanssen, A.M. Lempradl, J. Mauer, K. Timper, et al., IL-6/Stat3-dependent induction of a distinct, obesity-associated NK cell subpopulation deteriorates energy and glucose homeostasis, Cell Metab. 26 (1) (2017) 171–184, https://doi.org/10.1016/j.cmet.2017.05.018.
[36] S.W. Qian, Y. Tang, X. Li, Y. Liu, Y.Y. Zhang, H.Y. Huang, et al., BMP4-mediated brown fat-like changes in white adipose tissue alter glucose and energy homeostasis, Proc. Natl. Acad. Sci. U. S. A. 110 (9) (2013) E798–E807, https://doi.org/10.1073/pnas.1215236110.